



Na₂SO₄ + NaCl molten salts corrosion mechanism of thermal barrier coatings used in ships

Shuo Wu^{1,2} · Yuantao Zhao¹ · Wenge Li¹ · Weilai Liu³ · Yanpeng Wu⁴ · Zhongxian Zhao¹

Received: 31 October 2020 / Accepted: 2 February 2021 / Published online: 13 April 2021
© Akadémiai Kiadó, Budapest, Hungary 2021

Abstract

6–8 mass% Y₂O₃ stabilized ZrO₂ (6–8YSZ) thermal barrier coatings (TBCs) are widely applied to protect the hot ends of gas turbines in large navy ships. In this work, the 8YSZ TBCs were prepared by air plasma spraying technique, and their microstructure and phase composition were investigated. The hot corrosion mechanism of YSZ TBCs in molten salts consisting of 80% Na₂SO₄ + 20% NaCl at 900 °C was comprehensively analyzed. The results showed that the corrosion product Y₂(SO₄)₃ was formed due to the reaction between Na₂SO₄ media and the stabilizer Y₂O₃. As the result of the depletion of Y₂O₃ phase, the transformation from the tetragonal phase to monoclinic phase of ZrO₂ could not be totally inhibited, which consequently induced the 4–6 vol.% expansion and more cracks of YSZ TBCs. Meanwhile, the cracks could work as transfer paths for oxygen and molten salts. The kinetic analysis on hot corrosion also showed that more reaction products (from 2 to 8.1 mg cm⁻¹) were generated from 20 to 60 h due to more cracks generated by molten salts and oxygen infiltrating. More thermal grown oxides generated between ceramic layer, bonding layer and substrate, and the volume expansion caused by phase transition, increased the stresses in the coatings. Consequently, the peeling-off failure of 8YSZ TBCs could happen.

Keywords Thermal barrier coatings · Molten salts · Hot corrosion · Failure mechanism · Phase transformation

Abbreviations

YSZ	Y ₂ O ₃ stabilized ZrO ₂
TBCs	Thermal barrier coatings
SEM	Scanning electron microscope
EDS	Energy dispersive spectrometer
XRD	X-ray diffraction
T-ZrO ₂	Tetragonal phase ZrO ₂
M-ZrO ₂	Monoclinic phase ZrO ₂
C-ZrO ₂	Cubic phase ZrO ₂
Cps	Counts per second
APS	Air plasma spraying
TGO	Thermally grown oxides

Introduction

The navigable gas turbines with small volume and high single power are widely used in large warships such as cruisers, frigates and destroyers. However, with the continuous improvement of dynamic performance such as high speed and maneuverability, the inlet gas temperature of gas turbine is getting higher and higher, and challenging the performances of blade superalloy [1]. The air plasma sprayed 6–8 YSZ (6–8 mass% Y₂O₃ stabilized ZrO₂) have been used as TBCs materials commonly, which can reduce the adverse effects of high temperature on turbine blades superalloys [2–4]. However, the seawater salt spray (NaCl mainly) and turbine exhaust (containing SO₂, NO_x, V₂O₅) are easy to form corrosive salts (Na₂SO₄, NaVO₃, etc.) and accumulate on the surface of the coatings consequently in the high temperature ambient, resulting in the severe corrosion behaviors of the YSZ TBCs [5].

Recently, lots of scientific researches have focused on the corrosion behaviors of YSZ TBCs in hot molten salts deriving from the turbine exhaust. Among the salts, Na₂SO₄ and V₂O₅ mixtures have been used as the corrosion media to investigate the corrosion behaviors of the YSZ TBCs. Roche et al. [6] found that the rod-type and needle-shaped YVO₄

✉ Wenge Li
wgli@shmtu.edu.cn

¹ Merchant Marine College, Shanghai Maritime University, Shanghai 201306, China

² School of Construction Machinery, Shandong Jiaotong University, Jinan 250357, China

³ LNG Technology Research Institute, Hudong-Zhonghua Shipbuilding (Group) Co., Ltd., Shanghai 200129, China

⁴ Shanghai Rules and Research Institute, China Classification Society, Shanghai 200135, China

phases appeared on YSZ on account of the molten salt corrosion in high temperature ranging from 490 to 1100 °C, and the temperature strongly affected the corrosion mass loss of YSZ, and the major transformation of t-ZrO₂ took place at 900 °C. Besides, different mixing proportion of Na₂SO₄ + V₂O₅ would bring about different hot corrosion behaviors, the 32 mass% Na₂SO₄ + 68 mass% V₂O₅ mixed salts could lead to more phase-destabilization. Vaklifard et al. [7–9] revealed that the reaction between molten sulfate-vanadate salt and YSZ could consume the Y₂O₃ and generate the YVO₄, and simultaneously accelerate the phase transition of t-ZrO₂ to m-ZrO₂. This result also was verified by the works of Thakare et al. [10, 11], which also indicated that the addition of multiwall carbon nanotubes were detrimental to the corrosion behaviors of APS 8YSZ-Al₂O₃ TBCs. Qureshi et al. [12] confirmed that the t-ZrO₂ was transformed into m-ZrO₂ when YSZ TBCs were exposing in the molten salts Na₂SO₄ + V₂O₅ at 950 °C. Meanwhile, the spinel and perovskite structures were formed at the interface of topcoat (YSZ) and the bonding layer (NiCrAlY). Sivakumar et al. [13] found that the formation of YVO₄ facilitated the corrosion of YSZ in the molten salts containing V₂O₅, which was severer than the molten salts with Cl⁻. Hui et al. [14] also concluded that the 8YSZ coatings were easier to form m-ZrO₂ phases and produce rod-like YVO₄ when the coatings were corroded in Na₂SO₄ + 30 mol% NaVO₃ molten salts at 1100 °C.

In order to enhance the resistance of YSZ to molten salts, divers approaches have been explored and illuminated. For instance, designing double-ceramic-layer TBCs [15, 16], doping rare earth or alkaline earth oxide [17–19], laser glazing process [20], etc. However, the actual working ambient of YSZ TBCs was filled with not only turbine exhausts but also the sea salts like NaCl. Thus, the corrosion behaviors of YSZ TBCs in molten salts consisted of the turbine exhausts, and NaCl salt should be comprehensively explored. Ajay et al. [21] found that the formation of vertical cracks in YSZ TBCs could increase the strain tolerance and enhance the thermal cycling life. Whereas, they also worked as the diffusion paths for molten salts mixtures of Na₂SO₄ + V₂O₅ + NaCl at 900 °C to top layer/bonding layer interface, consequently accelerated the corrosion behaviors of coatings. Jonnalagadda et al. [22] prepared the composite coatings of Gd₂Zr₂O₇ + YSZ/YSZ and investigated the corrosion behaviors of the composite coatings in molten salts of 75 mass% Na₂SO₄ + 25 mass% NaCl at 900 °C. They suggested that the Gd₂Zr₂O₇ phases effectively obstructed the diffusion of molten salts and led to the aggregation of salts at the edges of the coating and severe corrosion at the edges. Although many explorations on the corrosion behaviors of YSZ in molten salts of Na₂SO₄ and NaCl have been made, the works are still insufficient, limiting the broad applications of YSZ TBCs. Especially, the comprehensive microstructure evolution and corrosion process of YSZ in

molten salts of Na₂SO₄ and NaCl need to be deeply investigated, which is meaningful and important for the applications of the YSZ TBCs.

Herein, the 8YSZ TBCs were prepared by atmospheric plasma spraying technique. The molten salts of Na₂SO₄ + NaCl at 900 °C were employed to investigate the hot corrosion behaviors of 8YSZ TBCs. The microstructure and phase composition of TBCs were comprehensively characterized before and after hot corrosion. Finally, the corrosion mechanism of Na₂SO₄ + NaCl to YSZ coating was analyzed.

Materials and methods

Materials, equipment and preparation methods

The TBCs system were prepared on the substrate of IN713C superalloys with sizes of 20 × 20 × 5 mm (provided by Shenzhen Malte Metal Materials Co., Ltd) by APS technique, which were composed of the NiCrAlY bonding layer and the 8YSZ ceramic layer. The thickness of NiCrAlY bonding layer and 8YSZ ceramic layer was ca 100 μm and 250 μm by adjusting the plasma spray times, respectively. The 8YSZ powders with the size of – 125 + 11 μm and the NiCrAlY powders with the size of – 106 + 53 μm were provided by Oerlikon Metco. The detailed composition of as-received powders is listed in Table 1.

Before preparing the coating, the surface of IN713C substrates was roughened by sand blasting for 5 min. Then, they were ultrasonically cleaned in ethanol for 10 min to remove the surface fragments and contamination. After that, a Metco UnicoatPro 7 M atmospheric plasma spray instrument was used to prepare the TBCs systems on IN713C alloys. In related research works [24, 25], the preparation parameters for the NiCrAlY bonding layer have been widely explored. After analyzing the research results above, the well-acknowledged parameters (the spraying power of 39 KW, spraying speed of 30 mm s⁻¹, Ar gas flow of 46 L min⁻¹, H₂ gas flow of 6 L min⁻¹, feeding rate of 28 g min⁻¹) were utilized to prepare the bonding layer. With respect to the 8YSZ top layer, the preparation parameters were selected from preliminary tests [26–28]. The spraying power was 35 KW, Ar gas flow was 32 L min⁻¹, H₂ gas flow was 8 L min⁻¹ and feeding rate was 45 g min⁻¹. In the hot corrosion experiment, the mixed salts solution of 80 mass% Na₂SO₄ + 20 mass% NaCl were selected and brushed on the TBCs. The TBCs with mixed salts were heated to 900 °C which was slightly higher than the melting point of salts (884 °C of Na₂SO₄ and 801 °C of NaCl). The total time of the corrosion experiment was 80 h which was

Table 1 Composition of the as-received NiCrAlY powders [23]

Element	Cr	Al	Y	Ni
Percentage (%)	22	10	1	67

equally divided into 8 cycles. A total of fifteen samples, with five for each group and three groups as a whole, were taken out to be weighed and recorded every ten hours.

Characterization of the TBCs system

TM3030 scanning electron microscope, a desktop scanning electron microscope, supplied by Tianmei Scientific Instrument Co., LTD, was used to analyse the micro morphology of TBCs. The element distribution in the micro area of TBCs was analyzed qualitatively and quantitatively combined with its auxiliary set of EDS. A multi-functional powder XRD analyzer, produced by Panalytical Co. in Holland, was used for phase analysis. The technical parameters are as follows, power 3 KW, scanning speed 5° min⁻¹, Cu K α radiation and diffraction angle $2\theta=5^{\circ}$ –100°. Software X'Pert Data Collector was employed to collect data, and Software X'Pert HighScore Plus was used for phase identification.

Results and discussion

Microstructure analysis before hot corrosion

The surface morphology of the TBCs is exhibited in Fig. 1. It is observed that the surface of the YSZ top layer is relatively flat with some cracks and semi-molten particles. The widths of the cracks were various, in which the large one can reach ca 0.5 μ m. These surface conditions of the sprayed YSZ were induced by the characteristics of air plasma spray technique. During plasma spray process of YSZ coatings, the semi-molten or molten state of the high-speed particle droplets was impinged on the surface of bonding layer on

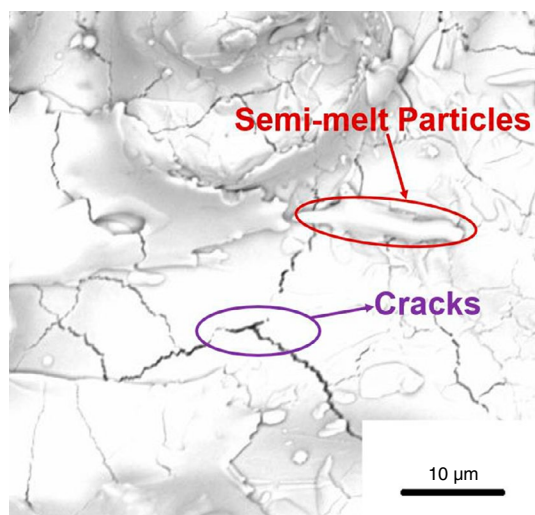


Fig. 1 The surface appearance of TBCs

the substrate, consequently forming some pores in the coatings. Meanwhile, the thermal stress and solidification stress could be formed as a result of the condensation shrinkage of the coating and the difference in the thermal expansion coefficient between top and bonding layers. The co-work of the stresses and pores led to the generation and propagation of cracks near the pores in the YSZ coating.

The cross-sectional morphology of the TBC system is shown in Fig. 2. It is observed that the cross section of the samples is consisted of three parts, which are YSZ top layer, NiCrAlY bonding layer and IN713C superalloy substrate. Lots of pores and cracks appear in both top layer and bonding layer. Whereas, the amount and size of the pores and cracks in top layer seem to be larger than those in bonding layer. The differences in flowability of molten ceramic and metal particles led to the different distribution of pores and cracks. The low melting point and high flowability of molten particles gave birth to the less pores and cracks in bonding layer. Moreover, the boundaries among these layers are not straight but fluctuant, consequently increasing the bonding strength among these layers.

EDS analysis before hot corrosion

The EDS energy spectrum was applied to analyse the composition distributions of TBCs along the red narrow direction as shown in Fig. 2. The results are exhibited in Fig. 3.

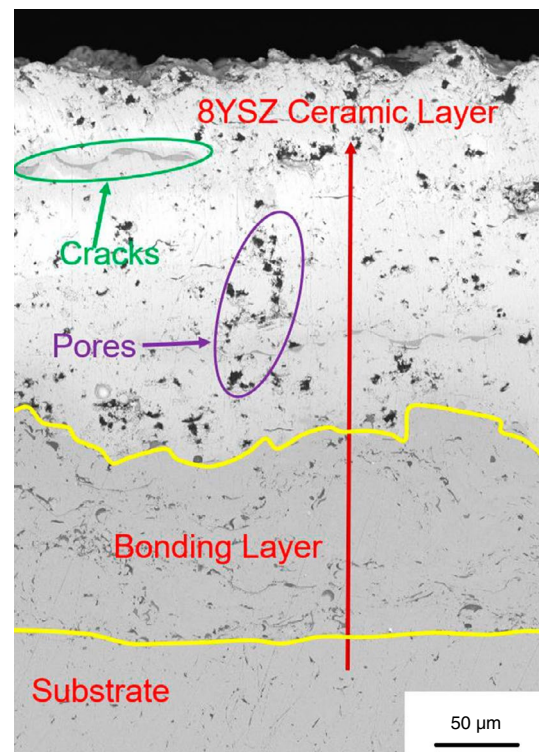
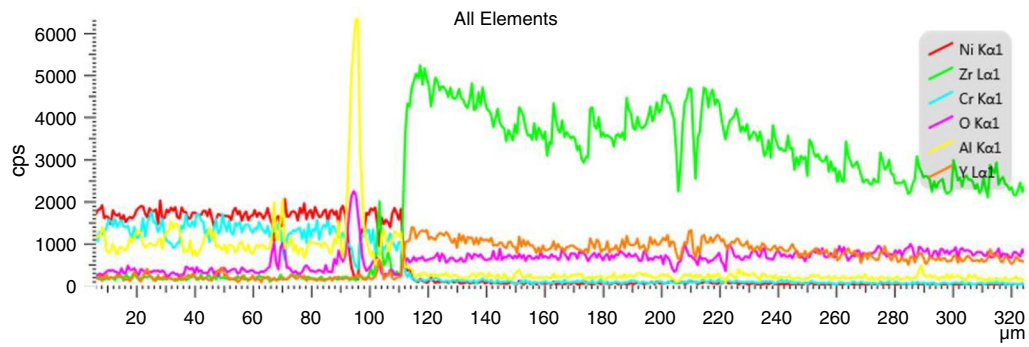
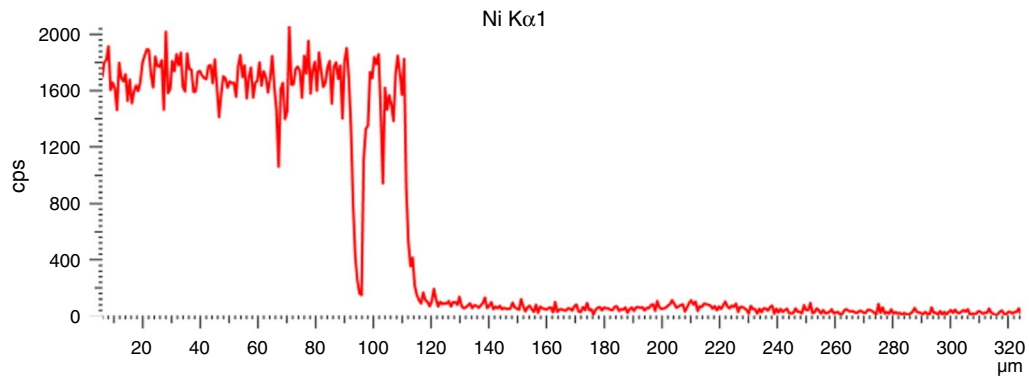


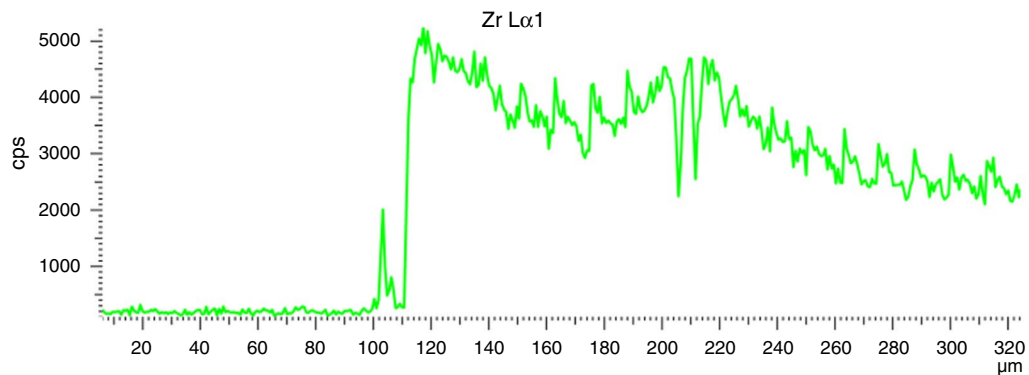
Fig. 2 The section morphology of TBCs



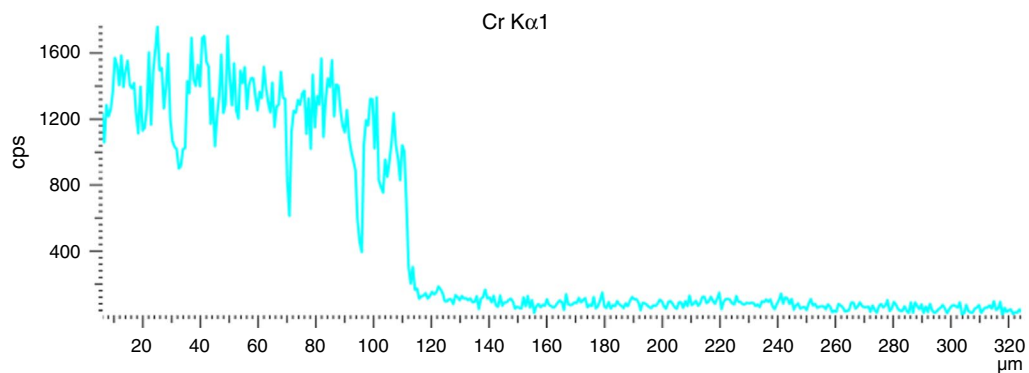
(a) Elements content strength change with distance



(b) Element Ni content strength change with distance



(c) Element Zr content strength change with distance

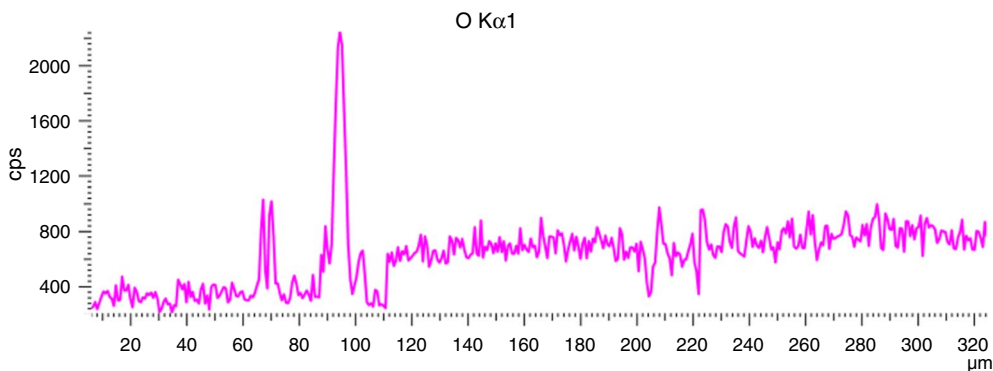


(d) Element Cr content strength change with distance

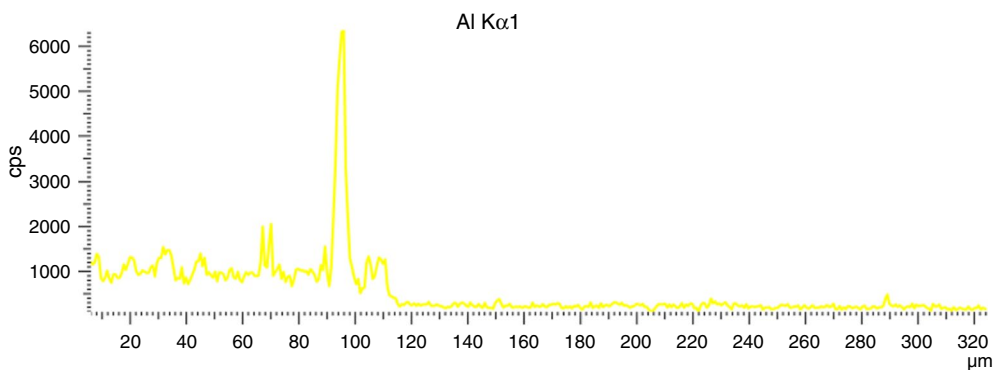
Fig. 3 Section EDS analysis of the thermal barrier coatings

It can be found that the distribution trend of element Zr is similar to that of element Y from the substrate to the surface, which is almost opposite to distribution of Cr, Ni and Al. This was caused by the composition difference of the layers. At the site of ca 110 μm, the sudden changes in distribution appear for all the elements, meaning this site as the boundary between YSZ and NiCrAlY layers. Taking a careful observation, some waves of distribution lines of Zr, Y and O elements can be found at the site of ca 210 μm, which indicates a pore or crack. At the site of

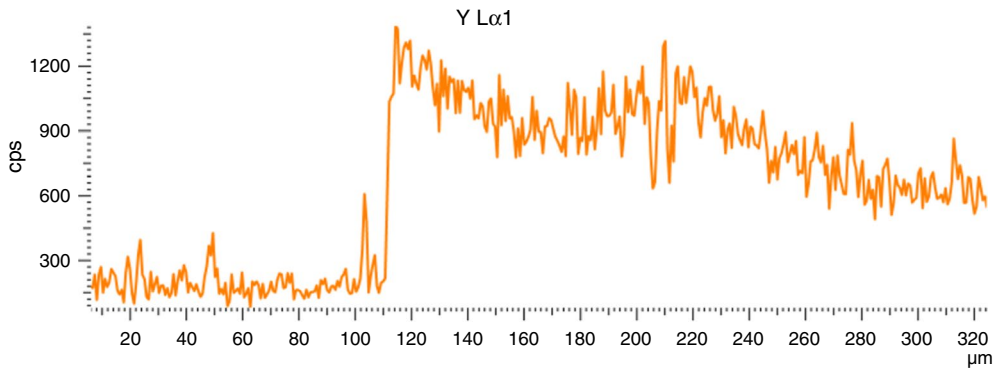
ca 102 μm, it is observed that the contents of Zr, Y and O increase and those of Ni, Cr and Al decrease in a small range, demonstrating the appearance of the YSZ particles. This was caused by the high-speed impact of the plasma sprayed molten YSZ particles into the NiCrAlY layer. Additionally, it can be found that the contents of Al and O are much high, and those of Ni and Cr are much low at the sites of ca 96 μm, demonstrating that some kind of alumina are formed here. The production of alumina seems to be derived from the selective oxidation of Al in the molten



(e) Element O content strength change with distance



(f) Element Al content strength change with distance



(g) Element Y content strength change with distance

Fig. 3 (continued)

feed particles of bonding layer. Therefore, from the element distribution, the thickness of the various layers, the pores/cracks and oxides can be directly figured out.

XRD analysis of the TBCs before hot corrosion

Figure 4 shows the phase composition of 8YSZ ceramic powder in XRD diffraction pattern. According to the analysis from the figure, 8YSZ ceramic powder particles were mainly consisted of t-ZrO₂ phase and Y₂O₃ phase. Besides, It can be seen that the diffraction peak of m-ZrO₂ phase of 8YSZ powder particles was very weak, so it was not marked in the figure.

Figure 5 shows the X-ray diffraction pattern of 8YSZ TBCs. It can be found that the main phase in sprayed 8YSZ coating is t-ZrO₂ phase with some Y₂O₃ phases. Compared with ceramic particle powders, the phases in the coating had an extra c-ZrO₂ phase, which was because a small amount of t-ZrO₂ in particles of 8YSZ ceramic powder had transformed into c-ZrO₂ at the high temperature after the plasma flame flow heating during the spraying process. Therefore, there existed c-ZrO₂ stabilized by Y₂O₃ in the coating. In the plasma spraying process, the powder particles were not uniformly heated in the high temperature and high-speed flame flow, leading to the lattice distortion of some ceramic powders, so the diffraction peak intensity decreased in the coating.

Microstructure of the high-temperature corroded coating

The surface morphology of 8YSZ TBCs after being corroded for 20, 40 and 80 h in molten salts of 80 mass% Na₂SO₄ + 20 mass% NaCl at 900 °C is shown in Fig. 6. It is observed that the content of molten salts colored by gray is reduced with

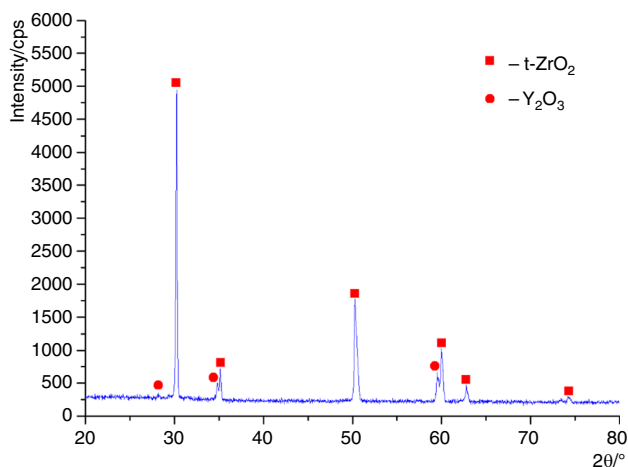


Fig. 4 XRD patterns of 8YSZ powder particles

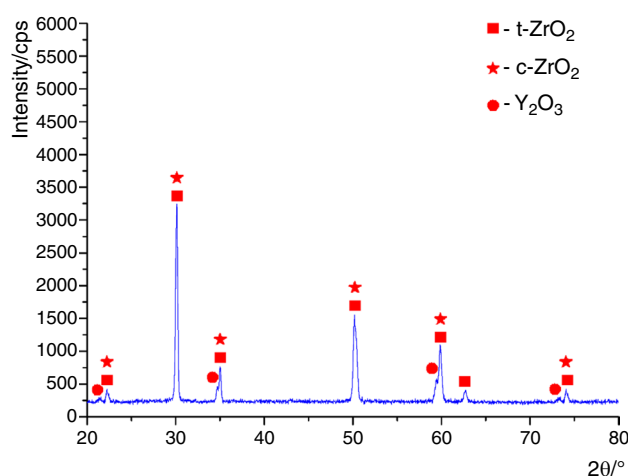


Fig. 5 XRD pattern of 8YSZ coatings

increasing the exposure time of the samples. Comparing to the surface morphology of the YSZ coating (as shown in Fig. 1), it is easy to find some larger-scale cracks appearing in the coating after hot corrosion, no matter 20, 40 or 80 h. Besides, the width and length of the cracks gradually increase as the hot corrosion time prolongs. Especially, the width of some large cracks after hot corrosion for 80 h can reach 5 μm.

The increase in the width of cracks was induced by the corrosion behaviors of the YSZ coating in molten salts of 80 mass% Na₂SO₄ + 20 mass% NaCl at 900 °C. As shown in Fig. 1, lots of cracks led to the penetration of the molten salts into the YSZ coating, consequently accelerating the hot corrosion of salts. Especially, the consumption of the Y₂O₃ would happen due to the corrosion reaction between the Y₂O₃ and molten salts. Subsequently, the stabilizer roles of Y₂O₃ for preventing the transformation of the t-ZrO₂ to m-ZrO₂ were weakened at 900 °C. The formation of m-ZrO₂ could increase the volume of the ZrO₂ phase, consequently increase the mismatch among ZrO₂ phases and increase the internal stress. In particular, lots of molten salts flowed into the cracks and pores, so that the Y₂O₃ near these sites could be severely depleted. As a result, the high volume changes and increased internal stress contributed to the development and propagation of cracks. With the hot corrosion time increasing, more molten salts could penetrate into the YSZ coating along cracks, which could be verified from the amount evolution of the gray substances in Fig. 6. Thus, more Y₂O₃ phases near cracks and pores were consumed, and the width of the cracks got larger. The width of the cracks was the largest in the YSZ coating after corroded in molten salts for 80 h.

Additionally, by the careful observation, it can be found that the surface of the YSZ coating after hot corrosion become more irregularity with more cracks, comparing to the coating before hot corrosion. This was induced by the consumption of Y₂O₃ phase in surface layer and the formation of the corrosion products.

The cross-sectional morphology of the TBCs after hot corrosion for 80 h is exhibited in Fig. 7. It is observed that lots of large-scale cracks and pores appear in the coating after hot corrosion. The length and width of cracks and pores apparently get larger comparing to the coating before corrosion as shown in Fig. 2. This was caused by the hot corrosion behaviors of YSZ coating in molten salts as discussed above. Besides, two obvious boundary areas appear between YSZ coating and bonding layer, bonding layer and IN713 superalloy, which are the TGO products of bonding layer. In molten salts, the corrosive salts could reach the surface of bonding layer via the cracks or pores, subsequently induced the chemical reaction of bonding layer derived from the combination of Cl, O elements and metal Al, Cr, etc. [22]. Meanwhile, some oxygen atoms from the hot air could also contribute to the formation of TGO. Especially, for the coating after corrosion for long time, the large-scale cracks and pores were more convenient for the infiltration of the molten salts. Thus, lots of TGO layers could be formed as shown in Fig. 7, which also increased the mismatch between YSZ and bonding layer and consequently brought into the propagation of more cracks. Meanwhile, owing to the porosity of bonding layer, some TGO products were also formed in interior of the bonding layer. The formation of TGO distinguished three evident layers in TBCs system as shown in Fig. 7, in which they were YSZ, bonding layer and substrate.

EDS analysis of TBCs after hot corrosion

Figure 8 shows the EDS spectrum analysis of TBCs system after hot corrosion at 900 °C for 80 h, which is the line scanning from the ceramic coating to the substrate as shown in Fig. 7. It can be found that the distribution of all the elements in the corroded TBCs is much different from that in the TBC before hot corrosion by comparing Fig. 3 with Fig. 8. In Fig. 8, by the scan in the opposite direction, the content of Zr element suddenly decrease at site of ca 160 μm, which

reversely and correspondingly happens at site of 110 μm with respect to the TBCs before corrosion. And the distribution evolution of Zr along EDS scanning direction is similar to that of Na, which greatly differs from others. Besides, in the site ranges from 160 μm to 300 μm, the distribution of almost all the elements fluctuated wildly. These distribution evolutions of elements were caused by the corrosion behaviors of Na₂SO₄ + NaCl and the formation of TGO products. During the hot corrosion of YSZ, the ever-increasing cracks and pores accelerated the diffusion of molten salts into the bottom of the YSZ coating, consequently brought in severe corrosion of YSZ and NiCrAlY bonding layer. Especially, the much severe corrosion of NiCrAlY layer came out after the corrosion of Al, Cr and Ni metals, which promoted the outwards diffusion of the metals. Meanwhile, the anions of molten salts solution like SO₄²⁻, Cl⁻ and some oxygen atoms inward diffused to attack the NiCrAlY due to the driving force of chemical corrosion, whereas the Na⁺ did not change a lot. Correspondingly, the sudden distribution change took place as the EDS line scanned across the TGO products in NiCrAlY layer in Fig. 7. Therefore, the corrosion behaviors and the TGO in TBCs system contributed to the element distribution evolution.

Phase composition of TBCs after hot corrosion

To analyse the phase evolution of the TBCs in hot corrosion, the phase composition of TBCs after hot corrosion for 80 h was measured by XRD. The XRD pattern is exhibited in Fig. 9.

As shown in Fig. 9, XRD pattern was made on the surface of 8YSZ TBCs after 80 h of high temperature corrosion. According to the analysis from the diffraction pattern, the surface phase of TBCs changed at 900 °C high temperature corrosion for 80 h, and a small amount of m-ZrO₂ appeared, which was probably caused by the decrease of the content of stabilizer Y₂O₃, due to the small amounts of chemical reaction with molten salts, as shown in Eqs. 1 and 2. T-ZrO₂ was still the main phase of 8YSZ ceramic layer, together with the previously existing Y₂O₃ phase. T-ZrO₂, Y₂O₃ and m-ZrO₂ appeared mainly in the coating after high temperature corrosion. Therefore, 8YSZ ceramic layer still maintained t-ZrO₂ phase after high-temperature corrosion at 900 °C.

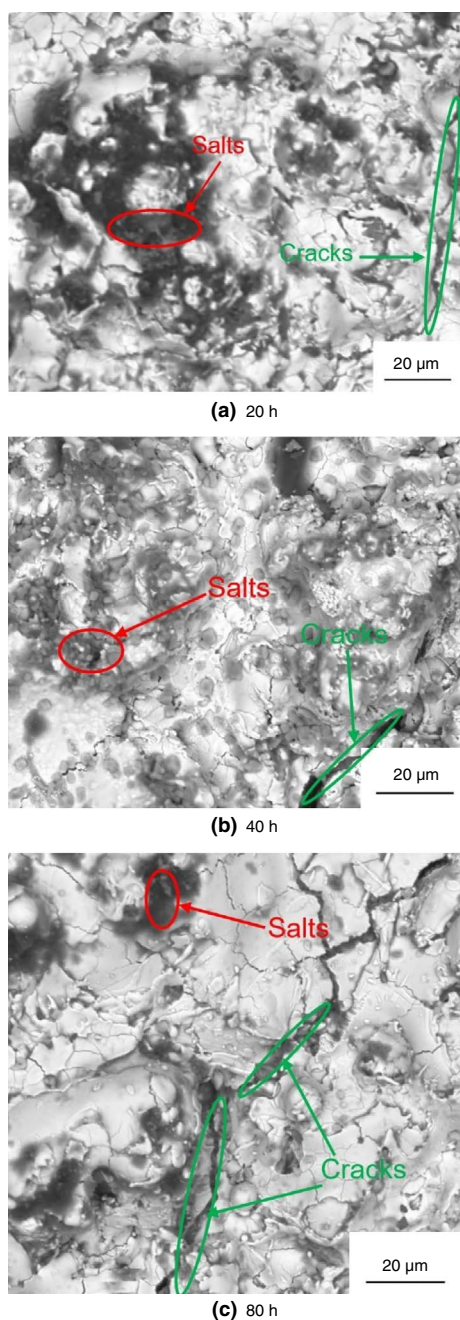
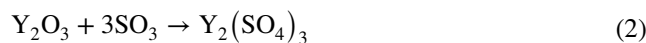


Fig. 6 Surface morphologies of YSZ TBCs after high temperature corrosion for different periods, **a** 20, **b** 40 and **c** 80 h

According to the theory of salt dissolution model established by Goebel et al. [29]. This model was established in molten salts, and could be shown in Eqs. 1 and 2.



The above reaction is unidirectional. With the forward progress of the reaction, Na_2SO_4 is decomposed into Na_2O and SO_3 , and SO_3 reacts with Y_2O_3 to generate $\text{Y}_2(\text{SO}_4)_3$. The two reactions promote mutually and will continue as long as the conditions are met. In 8YSZ TBCs, there is certain content of stabilizer Y_2O_3 and ZrO_2 . With the continuous progress of the above reaction, the content of stabilizer Y_2O_3 will gradually decrease. Y_2O_3 mainly plays a stabilizing role in TBCs to avoid the t- ZrO_2 in the coating transforming into m- ZrO_2 in high temperature environment. The $\text{Y}_2\text{O}_3 + 3\text{SO}_3 \rightarrow \text{Y}_2(\text{SO}_4)_3$ chemical reaction consumes the content of Y_2O_3 stabilizer and causes part of t-phase to be transformed into m-phase, which will be accompanied by 4–6% volume expansion of TBCs. The volume varying produced more cracks in coatings, which makes more oxygen infiltrate through these cracks onto the bonding layer, react with the metallic elements in the bonding layer and generate TGO consisting largely of Al_2O_3 . Thickening TGO layer increases the stresses between ceramic coating and bonding layer and eventually results in peeling-off of ceramic coating and failure of 8YSZ TBCs.

Kinetic analysis on hot corrosion

The mass evolution curve of 8YSZ TBCs with various hot corrosion periods in molten salts solution at 900 °C is shown in Fig. 10. It can be seen that the mass of the TBCs system gradually increases as the hot corrosion time increases. Having a careful observation, it can be seen that a slight increase in mass of TBCs occurs before 20 h. After that, the mass of TBCs gradually increases at a relative high rate with the hot corrosion time increases. Finally, the TBCs possess the largest mass increase after corrosion in molten salts for 80 h. In the period of rapid increase of corrosion products from 20 to

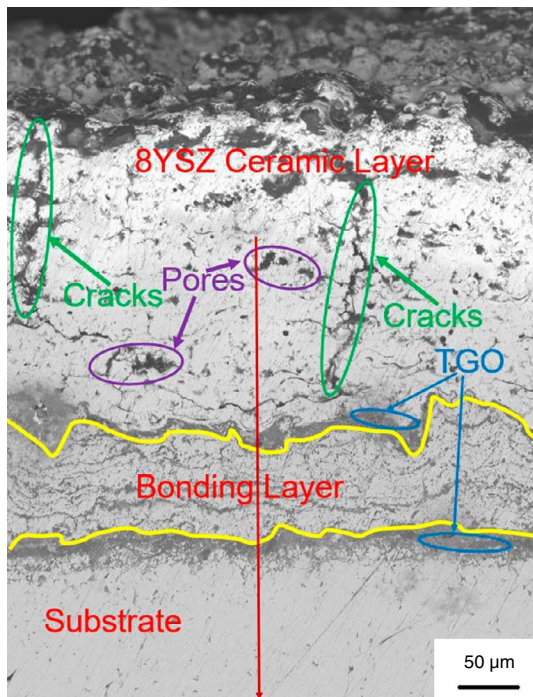


Fig. 7 Microstructure morphology of 8YSZ TBCs after 80 h high temperature corrosion

60 h, the mass change increases from 2 to 8.1 mg cm⁻², four times more than its original mass change. It is concluded that with the infiltration of more molten salts, some stabilizer Y₂O₃ is depleted, which results in the volume expansion and more cracks generating. As a result, more and more oxygen flows into TBCs and reacts with elements in the coatings. By the surface feature contrast of 8YSZ TBCs between Fig. 6a and b, it is also found that more salt-mixture enters into the pores, and the number of cracks is increasing. From

60 h later, the amount remains stable relatively, and the curve tends to be flat and stable. Basically, only a few more new corrosion products are generated. This is because that a majority of molten salts had infiltrated into the coatings after previous hot corrosion, the TBCs has been cracked, some stabilizer Y₂O₃ has been depleted by Na₂SO₄, and most exposed surfaces of TBCs have reacted with oxygen. Therefore, the formation rate of reaction production is getting slower.

The mass evolution of TBCs in corrosion ambient was attributed to the microstructure evolution and corrosion products of the TBCs system. As discussed above, the molten salts penetrated into the TBCs via the cracks and pores, consequently increased the mass of the TBCs. As corrosion time increased, more and more diffused molten salts could be consumed by the corrosion reaction between the molten salts and YSZ, NiCrAlY. This consumption contributed to the subsequent invasion of molten salts into the TBCs system. Furthermore, the scales of cracks and pores in the YSZ got larger with the increasing of corrosion time, which brought in the increased amount of molten salts into the TBCs system. Meanwhile, the molten salts could spread to the sites of new cracks, so that the scale of the new cracks increased due to the corrosion of molten salts. Furthermore, new cracks brought in more molten salts into the TBCs. Therefore, the continuous penetration of molten salts into TBCs and the gradually increased scales of cracks contributed to the mass increase of the TBCs system.

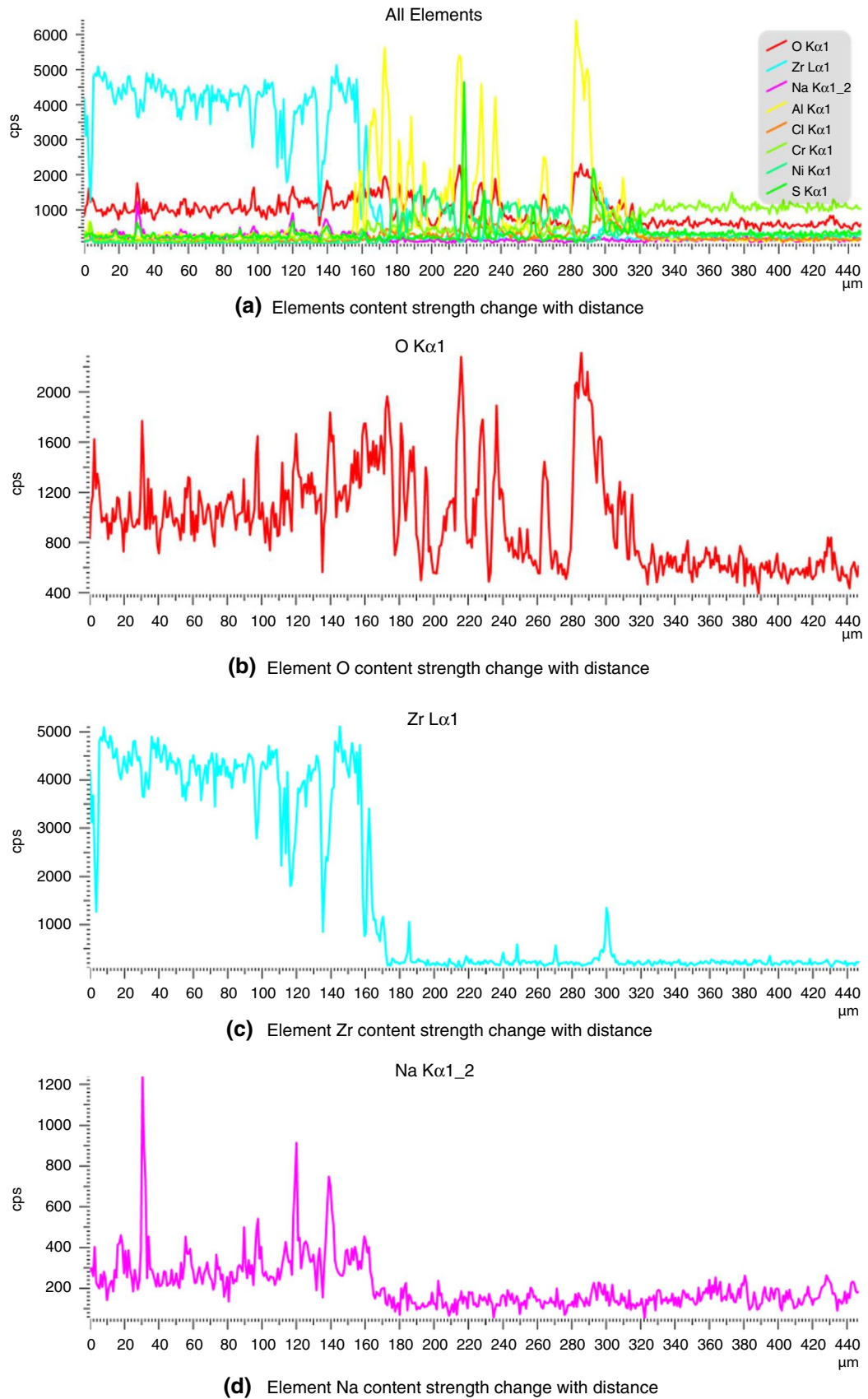
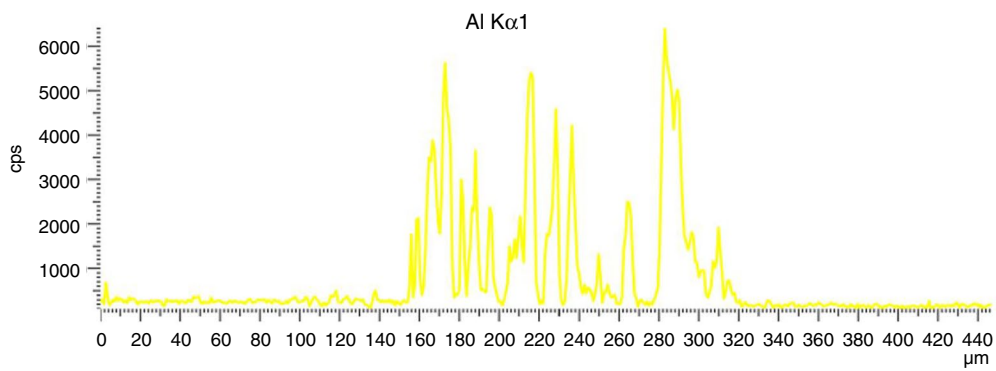
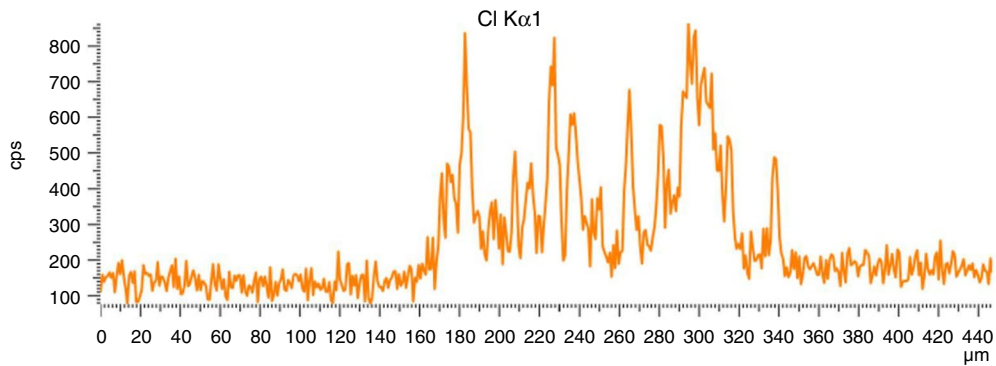


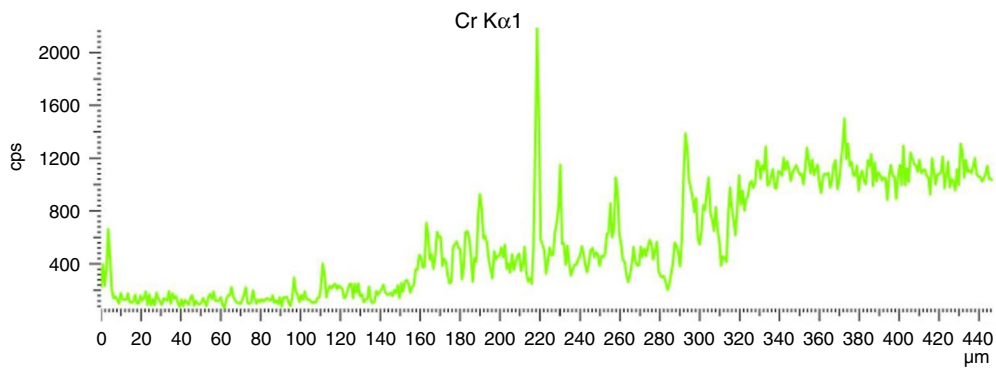
Fig. 8 Section EDS after high temperature corrosion of TBCs for 80 h



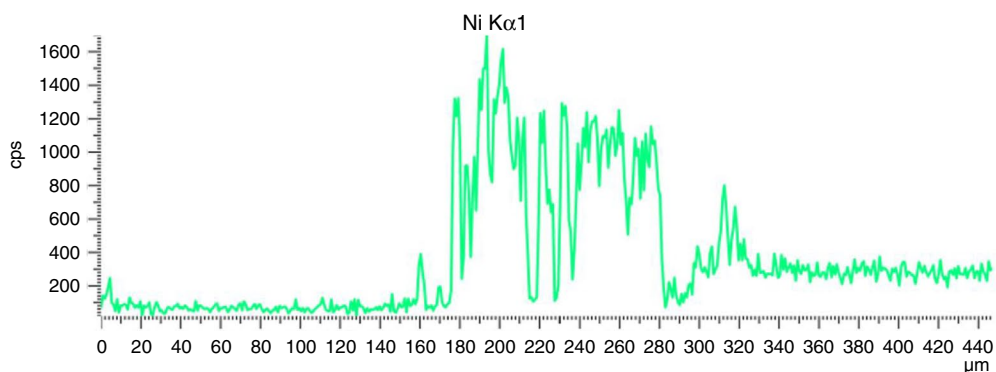
(e) Element Al content strength change with distance



(f) Element Cl content strength change with distance



(g) Element Cr content strength change with distance



(h) Element Ni content strength change with distance

Fig. 8 (continued)

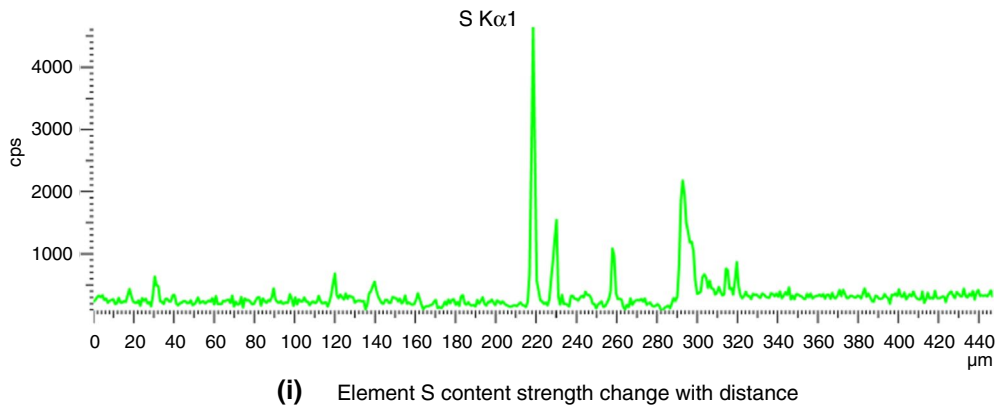


Fig. 8 (continued)

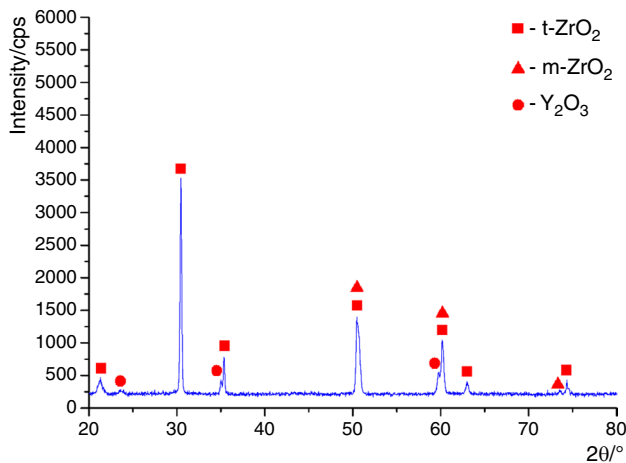


Fig. 9 XRD pattern of 8YSZ TBCs for 80 h thermal corrosion

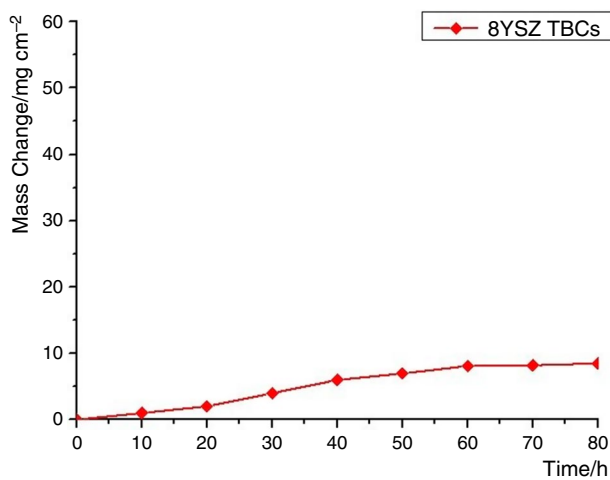


Fig. 10 Hot corrosion kinetics curve of 8YSZ TBCs at 900 °C

Conclusions

In this experiment, $\text{Na}_2\text{SO}_4 + \text{NaCl}$ molten salts corrosion mechanism of thermal barrier coatings was investigated. 8YSZ TBCs system was prepared on nickel-based IN713C superalloy by plasma spraying. The severe corrosion of TBCs system took place when they confronted with the molten salts of 80 mass% $\text{Na}_2\text{SO}_4 + 20$ mass% NaCl at 900 °C. The corrosion of the TBCs led to poor surface conditions and composition distribution evolution in TBCs. Especially, the corrosion behaviors of molten salts led to scale expansion including length and width of cracks and pores. With the increase of hot corrosion period, the scales of cracks and pores increased further.

The microstructure evolution of TBCs was caused by the consumption of Y_2O_3 phases and the formation of TGO in TBCs due to the corrosion reaction between Y_2O_3 , NiCrAlY and molten salts. As the results of the reaction between Y_2O_3 and molten salts, the transformation of $t\text{-ZrO}_2$ to $m\text{-ZrO}_2$ took place, subsequently brought in the volume changes of ZrO_2 phases and scale increasing of cracks and pores. The reaction between NiCrAlY and molten salts contributed to the formation of TGO and subsequently promoted the propagation of more cracks. Meanwhile, the increased scales of cracks and pores contributed to penetration of more molten salts and oxygen into TBCs, so that the scales of cracks and pores in YSZ TBCs gradually increased. Finally, the mass of TBCs got largest after 80 h hot corrosion as a result of the internal oxidation in the kinetic analysis on hot corrosion.

It is found that cracks in TBCs prepared by APS technique provide channels for molten salts penetration. Molten salts can react with stabilizer Y_2O_3 and bonding layer NiCrAlY , resulting in phase transition and volume change in TBCs and TGO growing on bonding layer,

generating stress and more cracks, and leading to failure of TBCs. The corrosion speed increases rapidly in the initial stage, and slows down with the increase of corrosion time. Protection measures, such as addition of protective film or protective elements, should be carried out to prevent YSZ TBCs from Na₂SO₄ + NaCl corrosion.

Author's contribution Conceptualization, WGL, WLL and SW; methodology, SW and Y TZ; software, SW; validation, WGL, Y TZ and SW; investigation, SW; data curation, SW, WLL, YPW and ZXZ; writing—original draft preparation, SW and WLL; writing—review and editing, SW, Y TZ and WGL; supervision, Y TZ and WGL; project administration, WGL; funding acquisition, WGL. All authors have read and agreed to the published version of the manuscript.

Funding This research was funded by special fund for green manufacturing system integration projects in 2018, the Ministry of Industry and Information Technology of China, key green process system integration of advanced turbine engine hot end components.

Data availability The datasets used or analyzed during the current study are available from the corresponding author on reasonable request.

Code availability Not applicable.

Compliance with ethical standards

Conflict of interest The authors declare no conflict of interest.

References

- Dychtoń K, Drajewicz M, Pytel M, Rokicki P, Nowotnik A. Ytria-stabilized zirconia–alumina composite sintering temperature effect on thermal diffusivity. *J Therm Anal Calorim.* 2016;126:1–7.
- Viswanathan K, Wang S, Esakkimuthu S. Impact of yttria stabilized zirconia coating on diesel engine performance and emission characteristics fuelled by lemon grass oil biofuel. *J Therm Anal Calorim.* 2020.
- Krishna Anand VG, Parammasivam KM. Thermal barrier coated surface modifications for gas turbine film cooling: a review. *J Therm Anal Calorim.* 2020.
- Moskal G, Mikuškiewicz M, Jasik A. Thermal diffusivity measurement of ceramic materials used in spraying of TBC systems: the influence of materials' morphology and (re)manufacturing processes. *J Therm Anal Calorim.* 2019;138:4261–9.
- Hong-bo Y, Yuan-sheng W, Xuan W, Qiang WU. Research progress of hot corrosion and protection technology of gas turbine under marine environment. *Surf Technol.* 2020;49:163–72.
- De la Roche J, Alvarado-Orozco JM, Toro A. Hot corrosion mechanism of yttria-stabilized zirconia powder in the presence of molten Na₂SO₄ + V₂O₅ salts. *Rare Met.* 2020.
- Vakilifard H, Ghasemi R, Rahimpour M. Hot corrosion behaviour of plasma-sprayed functionally graded thermal barrier coatings in the presence of Na₂SO₄ + V₂O₅ molten salt. *Surf Coat Technol.* 2017;326:238–46.
- Ozgurluk Y, Doleker KM, Karaoglanli AC. Investigation of the effect of V₂O₅ and Na₂SO₄ melted salts on thermal barrier coatings under cyclic conditions. *Anti-Corrosion Methods Mater.* 2019.
- Habibi MH, Wang L, Guo SM. Evolution of hot corrosion resistance of YSZ, Gd₂Zr₂O₇, and Gd₂Zr₂O₇+YSZ composite thermal barrier coatings in Na₂SO₄ + V₂O₅ at 1050 °C. *J Eur Ceram Soc.* 2012;32:1635–42.
- Thakare JG, Mulik RS, Mahapatra MM, Upadhyaya R. Hot corrosion behavior of plasma sprayed 8YSZ-alumina-CNT composite coating in Na₂SO₄–60% V₂O₅ molten salt environment. *Ceram Int.* 2018;44:21533–45.
- Thakare JG, Mulik RS, Mahapatra MM. Evaluation of cyclic hot corrosion resistance of plasma-sprayed composite coating in Na₂SO₄–60%V₂O₅ molten salt environment. *J Therm Spray Technol.* 2020;29:811–24. <https://doi.org/10.1007/s11666-020-01010-z>.
- Qureshi IN, Shahid M, Nusair-Khan A. Hot corrosion of Ytria-stabilized zirconia coating, in a mixture of sodium sulfate and vanadium oxide at 950 °C. *J Therm Spray Technol.* 2016;25:567–79.
- Sivakumar G, Banerjee S, Raja VS, Joshi SV. Hot corrosion behavior of plasma sprayed powder-solution precursor hybrid thermal barrier coatings. *Surf Coat Technol.* 2018;349:452–61.
- Hui Y, Zhao S, Xu J, Zou B, Wang Y, Cai X, et al. High-temperature corrosion behavior of zirconia ceramic in molten Na₂SO₄ + NaVO₃ salt mixture. *Ceram Int.* 2016;42:341–50.
- Fang Y, Cui X, Jin G, Liu E, Zhang D, Wen X, et al. Microstructural evolution and hot corrosion behavior of La_{0.8}Ba_{0.2}TiO₃–δ-YSZ double-layer thermal barrier coatings in Na₂SO₄ + V₂O₅ molten salt at 900 °C. *Surf Coatings Technol.* 2020;399:126175.
- de la Roche J, Gómez PA, Alvarado-Orozco JM, Toro A. Hot corrosion and thermal shock resistance of Dense-CYSZ/YSZ bilayer thermal barrier coatings systems applied onto Ni-base superalloy. *J Eur Ceram Soc.* 2020;40:5692–703.
- Bahamirian M, Hadavi SMM, Farvizi M, Keyvani A, Rahimpour MR. ZrO₂ 9.5Y₂O₃ 5.6Yb₂O₃ 5.2Gd₂O₃; a promising TBC material with high resistance to hot corrosion. *J Asian Ceram Soc.* 2020;8:898–908.
- Song D, Song T, Paik U, Lyu G, Kim J, Yang SC, et al. Hot-corrosion resistance and phase stability of Yb₂O₃–Gd₂O₃–Y₂O₃ costabilized zirconia-based thermal barrier coatings against Na₂SO₄ + V₂O₅ molten salts. *Surf Coatings Technol.* 2020;400:126197.
- Mohammadi M, Kobayashi A, Javadpour S, Jahromi SAJ. Evaluation of hot corrosion behaviors of Al₂O₃-YSZ composite TBC on gradient MCrAlY coatings in the presence of Na₂SO₄-NaVO₃ salt. *Vacuum.* 2019;167:547–53.
- Ahmadi MS, Shoja-Razavi R, Valefi Z, Jamali H. Evaluation of hot corrosion behavior of plasma sprayed and laser glazed YSZ–Al₂O₃ thermal barrier composite. *Opt Laser Technol.* 2019;111:687–95.
- Ajay A, Raja VS, Sivakumar G, Joshi SV. Hot corrosion behavior of solution precursor and atmospheric plasma sprayed thermal barrier coatings. *Corros Sci.* 2015;98:271–9.
- Jonnalagadda KP, Mahade S, Kramer S, Zhang P, Curry N, Li XH, et al. *J Therm Spray Technol.* 2019;28:212–22.
- Metco O. MCrAlY alloy. *Therm Spray Mater Guid V201704.* 2017. p. 13.
- Gildersleeve VEJ, Viswanathan V, Lance MJ, Haynes JA, Pint BA, Sampath S. Role of bond coat processing methods on the durability of plasma sprayed thermal barrier systems. *Surf Coat Technol.* 2019;375:782–92.
- Kane KA, Lance MJ, Sweet M, Pint BA. The effect of bond coating surface modification on the performance of atmospheric plasma spray thermal barrier coatings. *Surf Coatings Technol.* 2019;378:125042.

26. Tang R. Research on properties and process parameters of plasma sprayed 8YSZ thermal barrier coating. Jiangsu: Jiangsu University; 2019.
27. Guanggui C, Rongrong T, Cheng Y, et al. Study on the variation rules of thermal barrier coatings performance based on orthogonal experiment. *J Therm Spray Technol.* 2019;11:49–57.
28. Taijiang L, Erjuan Y, Wei L, Yong L, Gang L. Effects of preparation parameters on high temperature erosion properties of plasma sprayed thermal barrier coatings. *Mater Prot.* 2017;50:44–7.
29. Goebel JA, Pettit FS, Goward GW. Mechanisms for the hot corrosion of nickel-base alloys. *Metall Trans.* 1973;4:261–78.

Publisher's Note Springer Nature remains neutral with regard to jurisdictional claims in published maps and institutional affiliations.